2023

Rapid Detection of SARS-CoV-2 Nucleocapsid Protein by a Label-Free Biosensor Based on Optical Fiber Cylindrical Micro-Resonator

Ru-Lei Xia
Nanchang Hangkong University, China

Bin Liu
Nanchang Hangkong University, China

Yingying Hu
Nanchang Hangkong University, China

See next page for additional authors

Funder: National Natural Science Foundation of China; Natural Science Foundation of Jiangxi Province; Research and Development Projects of the Ministry of Science and Technology of China Number;Royal Society International Exchanges 2020 Cost Share (NSFNanchang Hangkong University Graduate Student Innovation Special Fund ProjeNational Natural Science Foundation of the China-Royal Society Exchange Program

Rapid Detection of SARS-CoV-2 Nucleocapsid Protein by a Label-free biosensor based on Optical Fiber Cylindrical Micro-resonator

Ru-Lei Xia, Bin Liu*, Yingying Hu, Juan Liu, Yue Fu, Xing-Dao He, Ping Lu, Gerald Farrell, Jinhui Yuan and Qiang Wu**

***Abstract*—The current global outbreak of coronavirus (COVID-19) continues to be a severe threat to human health. Rapid, low-cost and accurate antigen detection methods are very important for disease diagnosis. The severe acute respiratory syndrome coronavirus-2 (SARS-CoV-2) nucleocapsid protein (N-Protein) is often used as the diagnostic and screening for coronavirus detection. To this end, we propose and experimentally validate a highly sensitive whispering gallery mode (WGM) optical cylindrical micro-resonator (CMR) for bio-immunoassay detection. To study the biokinetic process of immunoassay, the surface of the WGM micro-resonator is functionalized with N-Protein monoclonal antibody (N-Protein-mAb), which led to the specific detection of N-Proteins. The spectral characteristics of the WGM resonance dip were investigated, it is found that the transmission spectrum of WGM shows a monotonically increasing red-shift as a function of recording time. The WGM red-shift is due to the antibody-antigen reaction and can be used for the analysis of the immunoassay process. The wavelength shift is shown to be proportional to the concentration of N-Protein, which ranges between 0.1 μg/mL and 100 μg/mL. Finally, different types of samples (concentration of 10 μg/mL of N-Protein) were prepared and tested to simulate the specificity of the sensor in the practical application environment. This method has the merits of rapid assay, lower expense, easy preparation, and miniaturization, which makes the sensor have potential for broad applications in the field of biochemistry and biomedical detection.**

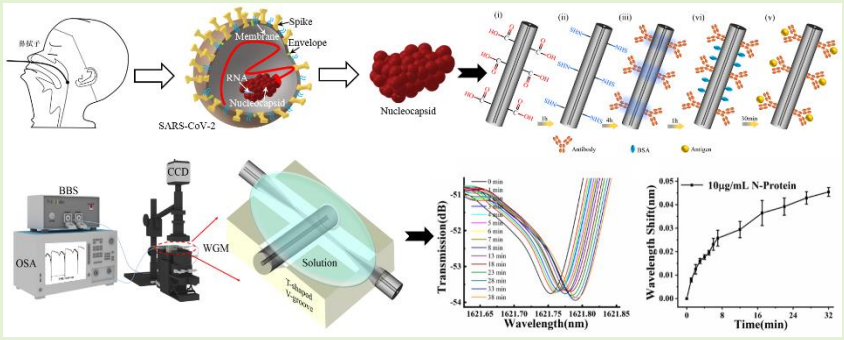

***Index Terms*—Optical fibre sensor; Whispering gallery mode (WGM); SARS-CoV-2 nucleocapsid protein (N-Protein); Biosensors**

I. Introduction

Currently, the cumulative number of confirmed cases of novel coronavirus 2019 (COVID-19, SARS-CoV-2) worldwide exceeds 500 million, and the number of deaths exceeds 6.5 million[1-5]. The continued spread of the disease and the emergence of new coronavirus variants has led to an unprecedented global research effort to combat this devastating outbreak. Currently, it is known that the main structural proteins of neo-coronavirus include spike protein (S-Protein) [6-10], envelope protein (E-Protein), membrane protein (M-Protein) and nucleocapsid protein (N-Protein) [11-13].

A large amount of attention in neo-coronavirus drug and vaccine research has focused on the S-Protein that directly mediate neo-coronavirus infection of human cells. As the understanding of neo-coronaviruses has become more advanced, other important roles of neo-coronavirus proteins have been revealed, including the N-Protein that helps transcribe and replicate viral RNA in the host cell.

The N protein is the most abundant viral structural protein during neo-coronavirus infection and is abundantly expressed after the virus infects human cells, causing a strong immune response. The N-Protein is often used as a diagnostic test for coronaviruses and is a core ingredient in immunological rapid diagnostic reagents.

Since the outbreak of COVID-19, there has been a huge drive globally to develop innovative detection technology as a key element of successful epidemic prevention and control. Fiber sensors have been shown to possess a wide range of advantages and have demonstrated exceptionally high detection sensitivity in a number of areas such as bio-sensing, medical diagnostics, human health monitoring and biological detection [14].

This work was jointly supported by National Natural Science Foundation of China (NSFC) (62175097 and 62065013); Natural Science Foundation of Jiangxi Province (Grant No. 20212BAB202024); Key R&D Projects of the Ministry of Science and Technology of China (2018YFE0115700); Royal

Society International Exchanges 2020 Cost Share (NSFC) (IEC\NSFC\201015); Nanchang Hangkong University graduate student innovation special fund project (Grant No. YC2021-074) and National Natural Science Foundation of China-Royal Society Exchange Programme (62111530153). (Correspondence authors: Bin Liu and Qiang Wu)

Ru-Lei Xia, Bin Liu, Yingying Hu, Juan Liu, Yue Fu, Xing-Dao He and Qiang Wu are with Key Laboratory of Opto-Electronic Information Science and Technology of Jiangxi Province, Nanchang Hangkong University, Nanchang 330063, China (e-mail: m17730173360@163.com; liubin@nchu.edu.cn; yyhu@nchu.edu.cn; 18042@nchu.edu.cn; 71212@nchu.edu.cn; hxd@nchu.edu.cn; qiang.wu@northumbria.ac.uk).

Qiang Wu is also with Faculty of Engineering and Environment, Northumbria University, Newcastle Upon Tyne NE1 8ST, UK.

Ping Lu is with School of Optical and Electronic Information, Huazhong University of Science and Technology, Wuhan 430074, China (pluriver@mail.hust.edu.cn).

Gerald Farrell is with Photonics Research Centre, School of Electrical and Electronic Engineering, City Campus, Technological University Dublin, Dublin 7, Ireland (gerald.farrell@TUDublin.ie).

Jinhui Yuan is with the Research Center for Convergence Networks and Ubiquitous Services, University of Science & Technology Beijing, Beijing 100083, China. (e-mail: yuanjinhui81@163.com).

A wide variety of different fiber types and structures have been investigated for sensing, for example those based on singlemode-multimode-singlemode fiber structures (SMS) [15], D-Shaped plastic optical fiber [16] and a tapered single-mode-coreless-single-mode coupler (tapered SNSFC) [17]. Interferometric techniques have also been employed, for example a side-Polished single-mode Fiber Mach-Zehnder Interferometer [18]. Recently in 2021, M. Divagar *et al* [19]. proposed a plasmonic fibre absorbance biosensor (P-FAB) for the clinical detection of N-protein, which is present in abundance during infection. P-FAB utilizes a sandwich detection technique with the plasma of the labels on the surface of a U-shaped bend fibre sensor probe, which results in the limit of detection (LoD) down to ~2.5 ng/mL. H. Jia *et al* [20] reported a novel method to detect the N-Protein by DNA/RNA oligomers as aptamers in combination with a graphene oxide (GO) coated microfiber, with lowest LoD of 6.25×10^{-19} M. Very recently D.K. Agarwal *et al* [21] reported an optical detection sensor based on microcantilever for SARS-CoV-2 antigenic proteins. The sensor employed a fluidic-atomic force microscopy (f-AFM) mediated nano-mechanical deflecting approach. Using this sensor, rapid detection of N-Protein and spike (S1) receptor binding domain (RBD) proteins was first proved at a clinically pertinent concentration as low as 1 ng/mL (33 pM) by detecting of the nano-mechanical signal elicited with antibody-antigen binding.

WGM optical micro-resonators have been shown to be a viable platform for developing biological sensors [22–24]. WGM based sensors are very compact, relatively easy to integrate with other devices, possess strong biocompatibility and superior resistance to electromagnetic interference (EMI). WGM microresonant cavities rely on small mode sizes and offer high q-factors in light-matter interactions. They are also very sensitive to temperature [25], humidity [26], hydrogen [27], and biomolecular substances such proteins [28], nucleic acid [29], antigen or antibody [30], and phage [31].

In the paper, a high-sensitivity and high-specificity optical cylindrical micro-resonator (CMR) sensor suitable for bio-immunoassay for COVID-19 is presented and experimentally validated. The WGM CMR system utilizes a tapered single-mode optical fiber to couple the CMR. The biokinetics of the antigen-antibody reaction after functionalization of the CMR surface by N-Protein-mAb was studied to specifically detect the presence of N-Protein. The immunodetection detection of biological proteins is achieved by recording the changes of transmission spectra of the presented WGM optical CMR. The presented biosensor shows good reproducibility and specificity and has a wide range of applications in the fields of clinical medicine, disease diagnosis and drug screening.

II. Theoretical Background

It is well known for a CMR that WGMs arising from self-interference in the light circulating. A resonant state with a high Q-factor can be generated in the peripheral region of the microcylinder, which is distributed along the axial direction, as illustrated in Fig. 1. CMRs have the advantage that alignment for optimum coupling to the fiber resonator of the light relies on merely one angle degree of freedom, whereas more complex spherical structure has two degrees of freedom.

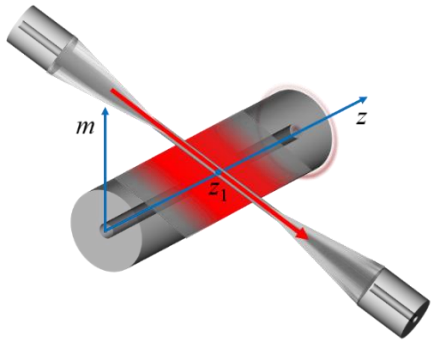

Fig. 1 Schematic diagram of microfiber waveguide coupling to the CMR (the red area represents the diffracted beam).

A circulating light beam that is evanescently coupled into the cylinder and experiences total internal reflection radiates out along the cylinder axis, which is defined as the characteristic width of WGM mode. At the resonance, the characteristic width is expressed as $(\alpha\beta)^{-1/2}$, where α and β are the attenuation and propagation constants of the CMR material [32].

The input microfiber mode $E_0(z, m, s)$, evanescently penetrates into the CMR. The resulting cycle WGM can be expanded into a linear combination of modes $G_{\mathrm{ml}}(z, m, s)$ with Hermite–Gaussian z components [33]:

$$\begin{aligned} G_{\mathrm{ml}}(z,m,s) &= q(s)^{-m/2} H_m\left(\beta_0^{1/2} z / q^{1/2}(s)\right) G_{0l}(s,z,m) \\ G_{0l}(z,m,s) &= q(s)^{-1/2} \exp\left[i(\beta_0 + i\alpha - \varsigma_l)s\right] \\ &\quad \times \exp\left(-\beta_0 z^2 / q(s)\right) \\ q(s) &= \eta + 2is \end{aligned} \tag{1}$$

Figure 2(a) illustrates the coordinate system used, where (s, z, m) are the azimuthal, radial, and axial coordinates. In the analysis $\beta_0=2\pi n_c/\lambda$, where β_0 is the transverse propagation constant, λ is the radiation wavelength and nc is the refractive index (RI) of the CMR. The term α is the attenuation constant

of the CMR and η is a free parameter. The term ς_l is associated with the transverse component of a beam.

The mode $E_0(z, m, s)$ and $G_{ml}(z, m, s)$ are coupled to each other. Here we are concerned with the behavior of mode $G_{ml}(z, m, s)$ after multiple circulations, $N \gg 1$, which can contribute to a high-Q-factor resonance. In terms of Eq. (1), for increasing s that corresponds to $N \gg 1$, the value of $G_{ml}(z, m, s)$ decreases as $s^{-(m+1)/2}$. Similar to a ring resonator [34] [shown in Fig. 2(b)], by CMR and microfiber coupling the transmission of resonance is denoted as the total of partial amplitudes:

$$\begin{aligned} n(\Delta\beta) &= n_{00}^{(0)} + n_{01}^{(1)}\exp\left[(i\Delta\beta - \alpha)s_0\right]n_{10}^{(1)} \\ &+ n_{01}^{(1)}\exp\left[(i\Delta\beta - \alpha)s_0\right]n_{11}^{(1)}\exp\left[(i\Delta\beta - \alpha)s_0\right]n_{10}^{(2)} + \cdots \\ &+ n_{01}^{(1)}\exp\left[(N+1)(i\Delta\beta - \alpha)s_0\right]n_{10}^{(N+1)}n_{11}^{(1)}n_{11}^{(2)} \ldots n_{11}^{(N)} + \cdots \end{aligned} \quad (2)$$

where $\Delta\beta = \beta - \beta_m$, where the resonance eigenvalue β_m is is defined by the formula $(\beta_m - \varsigma_l)R = m, m \gg 1$. In Eq. (2), $n_{ij}^{(N)}$, $i, j = 0,1$, are the amplitudes of direct coupling between the mode $E_0(z, m, s)(i, j = 0)$ and $G_{0l}(z, m, s)(i, j = 1)$ for the Nth circulation, i.e., near $s \approx Ns_0 = 2\pi NR$ [35]. In resonant transmission, the undercoupled state is reasonable, $\alpha s_0 \gg \left|n_{10}^{(1)}\right|^2$, The CMR intrinsic loss is greater than the coupling loss, which is determined by the material loss of α. Replacing $n_{10}^{(1)} = -\left(n_{01}^{(1)}\right)^*$, $n_{00}^{(0)} \approx 1 - \frac{1}{2}\left|n_{10}^{(1)}\right|^2$, and $n_{10}^{(N)} = n_{10}^{(1)}N^{-1/2}$ into Eq. (2) which yields the transmission power in the vicinity of the resonance is obtained:

$$\begin{aligned} P_{\text{cyl}}(\Delta\beta) &= |n(\Delta\beta)|^2 \underset{|\Delta\beta s_0|, |\alpha s_0| \ll 1}{\approx} \\ &1 - \left|n_{01}^{(1)}\right|^2 - 2\left|n_{01}^{(1)}\right|^2 \text{Re}\left\{\int_0^\infty \frac{dN}{N^{1/2}}\exp\left[(i\Delta\beta - \alpha)s_0 N\right]\right\} \end{aligned} \quad (3)$$

Ignoring the comparatively smaller nonresonant term $\left|n_{01}^{(1)}\right|^2$ in the right side of Eq. (3), which is expressed by calculating as [36]:

$$P_{\text{cyl}}(\Delta\beta) \approx 1 - \left|n_{01}^{(1)}\right|^2 \left[\frac{(\Delta\beta^2+\alpha^2)^{1/2}+\alpha}{R(\Delta\beta^2+\alpha^2)}\right]^{1/2} \quad (4)$$

The lorentzian transmission resonance of a CMR is defined by Eq. (4). and FWHM is related to $|\Delta\beta|$.

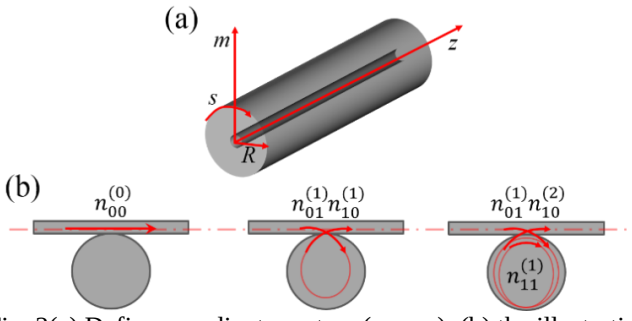

Fig. 2(a) Define coordinate system (z, m, s); (b) the illustration of terms in Eq. (2).

III. Fabrication of the Sensor

A short section (7 cm) of single-mode optical fibre (SMF-28e) was used as an optical CMR. The coating on the fibre was removed and then pre-treated with a flame brushing technique to ensure a smooth surface, this is necessary in order to allow efficient low loss evanescent coupling to take place between the CMR and the tapered fibre. Given the specification of the SMF-28e fiber used, all of the CMRs fabricated had a diameter of 125 µm ± 0.7 µm. The tapered microfibre (diameter of 2.76 µm) is prepared using a ceramic micro-oven (E-Otron, China) and a motion control setup to progressively taper the SMF-28e fiber. The tapered fiber is encapsulated with UV adhesive on a thin plate U-frame, which couples it to the CMR on a three-dimensional operating platform. Figure 3 shows a photograph of the constructed CMR and coupling system taken by a CCD camera, looking down on the CMR.

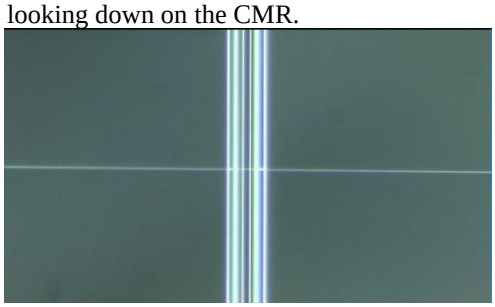

Fig. 3 Top perspective photo of WGM coupling system taken by CCD camera.

A schematic diagram of the experimental device established for fiber tapered waveguide coupling is illustrated in Fig. 4 (a). A broadband light source (BBS, FiberLake) was used, which had a spectral range of 1250 nm-1650 nm, the coupling structure between a CMR and the tapered fiber waveguide is observed by a CCD camera, and an optical spectrum analyzer (OSA, yokogawaAQ6370D) was used to detect the spectrum of the light coupled out of the micro-resonator into the tapered fibre. Figure 4(b) shows a schematic diagram of the coupled detection using the V-grooves combination, the tapered fibre and micro-resonator were held in alignment using customized 3D printed V-grooves, arranged at ninety degrees to each other. Light generated is coupled into the micro-resonator through a fibre tapered waveguide, and a transmission spectrum is obtained at the output. The total reflection phenomenon exists when the light propagates from the light-dense medium to the light-sparse medium, which can be used to completely confine the light inside the micro-resonator and form a stable WGM. When the total reflection of light occurs on the surface of the micro-resonator, a evanescent wave is formed on the surface, so that a tiny range of biomolecules can be measured. The WGM-based markerless optical biosensor is essentially a RI sensor, and the presence of the evanescent field causes the effective RI of the micro-resonator to change with the object to be detected outside the micro-resonator, which in turn causes a shift in the resonance wavelength.

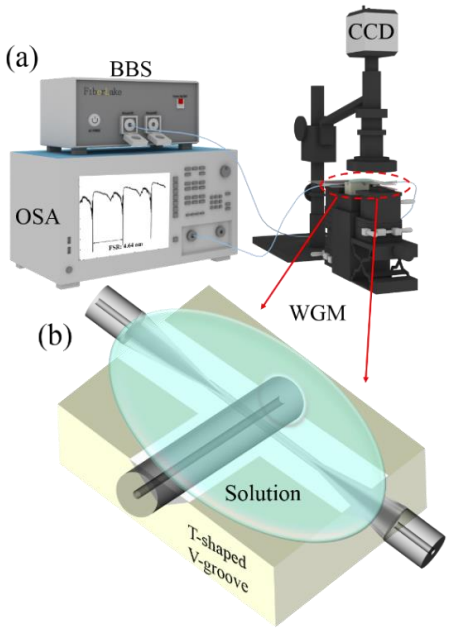

Fig. 4(a) Schematic diagram of the tapered fibre waveguide coupling experimental system; (b) schematic diagram of the V-groove arrangement used to align the CMR and tapered fibre.

The full width at half maxima (FWHM) of the WGM induced transmission spectral dip for the cylindrical micro-resonator was estimated using a Lorentzian fit as approximately 0.0284 nm at 1607 nm. Similarly, the FSR expression for wavelength can be obtained as: $FSR_\lambda = |\lambda_{m+1} - \lambda_m| = \frac{\lambda^2}{2\pi R n_{eff}}$. Here, the effective refractive index n_{eff} is 1.4628, the radius R is 62.5 μm, and the theoretically calculated FSR is 4.50 nm. In biosensing experiments, a large FSR is generally expected to increase the detectable range for sensing applications and the FSR obtained from the spectrum is 4.64 nm, which agrees well with the theoretical calculation result (4.50 nm). The Q-factor is a critical performance parameter for a resonator used as a sensor as it has a strong influence on the achievable detection sensitivity. Using the linewidth method, the Q value is estimated to be 5.66×10^4 as shown in Figs. 5(a) and (b).

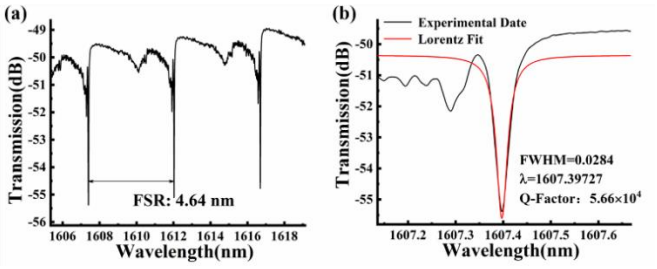

Fig. 5 (a) transmission spectrum of the CMR coupling; (b) Lorentz fit and its Q value.

IV. Experimental Results

Initially the spectral shift versus the surrounding RI characteristic for the resonator was measured. For this purpose, liquids with different RI values under different volume ratios of a mixture of dimethyl sulfoxide (DMSO) and deionized water were calibrated using an Abbe refractometer. The CMR was immersed in deionized water and the DMSO solution was added drop by drop, and the wavelength shift was recorded by OSA, as shown in Figure 6(a). The RI sensitivity of the CMR was found to be 72.48 nm/RIU with correlation coefficient (R^2) of 0.99, as shown in Figure 6(b).

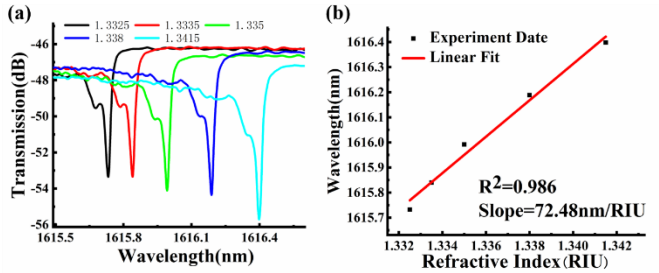

Fig. 6(a) Transmission spectrum of RI sensing of CMR cavity; (b) Fitting results of wavelength variation with refractive index.

The detection limit (DL) of a sensing system can be calculated as [37]:

$$\mathrm{DL} = \frac{3\sqrt{\sigma^2_{\text{ampl-noise}} + \sigma^2_{\text{temp-induced}} + \sigma^2_{\text{spect-res}}}}{S} \quad (5)$$

where S is the sensitivity to refractive index, $\sigma_{\text{ampl-noise}}$, $\sigma_{\text{temp-induced}}$ and $\sigma_{\text{spect}-\text{res}}$ are the mean square amplitudes of the system noise, thermal fluctuations and spectral resolution of the system, respectively. The $\sigma_{\text{temp-induced}}$ is generally small enough to be ignored. For the noise and spectral resolution terms:

$$\sigma_{\text{ampl-noise}} \approx \frac{FWHM}{4.5\times(OSNR)^{0.25}} \quad (6)$$

$$\sigma_{\text{spect}-\text{res}} = \frac{R_W}{2\sqrt{3}} \quad (7)$$

where the optical signal-to-noise ratio (OSNR) can be estimated from the extinction ratio of the interference spectrum, as approximately 6 dB, R_W is the wavelength scanning resolution of the OSA, which is 0.02 nm [38]. In our experiment, the FWHM and S are 0.0284 nm and 72.48 nm/RIU, respectively. The calculated DL is thus 2.9×10^{-4} RIU using Eq. (5).

To implement N-Protein sensing, the CMR is functionalized with N-Protein-mAb, which is a kind of antibody that will specifically bind to N-Protein. Once the antibody N-Protein-mAb is fixed on the surface of the CMR, the N-Protein will combine with the antibody N-Protein-mAb. The process of the binding can change the surrounding effective RI of the CMR, which will result a detectable resonant wavelength shift. When the wavelength shift has the corresponding regulation with the N-Protein concentration, it illustrates that the functionalization of CMR can be implemented for N-Protein detection.

Before functionalizing the sensor, the CMR was initially immersed into a standard solution of potassium hydroxide (KOH) for 1 hour and washed it with deionized (DI) water at least three times until neutral (pH=7). The CMR was then dried in the ambient environment. After cleaning the CMR is functionalized using the following sequence of steps below and also described in Fig. 7:

i. To generate the carboxyl: the sensor is immersed into silane reagent solution (3-(Triethoxysilyl) propylsuccinic anhydride, 5%) for 4 hours. The 5% silane reagent solution is obtained by mixing the 95% silane reagents and 99.5%

ethanol solution. This process generates carboxyl on the sensor's surface.

ii. Activated succinimide esters on the fiber surface is formed by the reaction of EDC with NHSS: An ethanol and phosphate buffer solution (PB, pH = 6.0) is used to wash the CMR and eliminate the residual silane reagent solution. The CMR is then treated by immersion for 1 hour in a mixture solution containing 1-(3-Dimethylaminopropyl)-3-ethylcarbodiimide hydrochloride (EDC, 0.8 mg/mL) and N-Hydroxysulfosuccinimide sodium salt (NHSS, 1.2 mg/mL). This step is performed to produce the succinimidyl ester.

iii. Antibody fixation: The CMR is washed with Phosphate Buffer Saline (PBS; (1X) .0067M (PO_4)) solution to clean the residual EDC and NHSS, and immersed in a 100 µg /mL solution of anti N-Protein-mAb (Beijing Bersee Science and Technology Co. Ltd.) for 4 hours.

iv. Nonspecific binding interruption: the antibody immobilized CMR was first washed for two times with PBS and then immersed with Bovine serum albumin (BSA, 1%) solution for 1 hours. It is a process that can be performed to suppress nonspecific binding of vacancies on the functionalized fiber surface.

v. The CMR was washed for two times with PBS after the BSA and used for N-Protein detection.

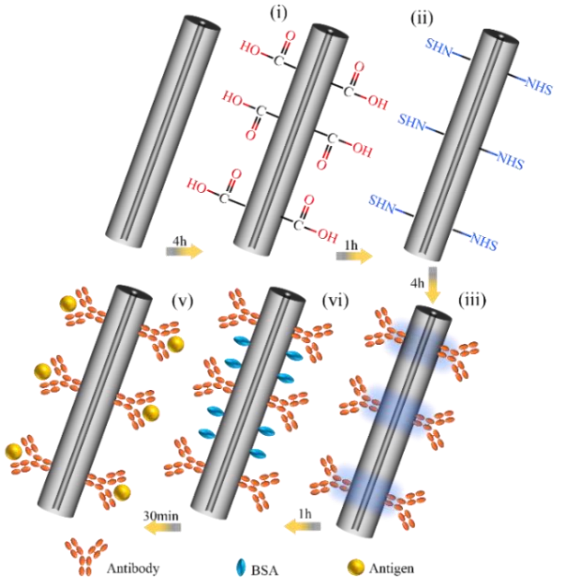

Fig. 7 The process of fixation anti N-Protein-mAb on the surface of a CMR is illustrated: (i) forming carboxyl; (ii) activation of succinimide ester; (iii) antibody fixation; (iv) nonspecific binding interruption; (v) detecting of specific binding SARS-CoV-2 N-Protein.

After functionalization, for reference the stability with time of the CMR was tested with a blank PBS solution before starting the measurements. The result of this are shown in Figure 8(a). This test took place over 30 minutes and was repeated four times. The maximum wavelength change lies within the range ±0.005 nm, which indicates that the developed CMR had good intrinsic stability.

It is important to note that immersion of the micro-resonator in a liquid will result in a large light absorption and thus the OSNR of the WGM spectrum will decrease significantly. This is unavoidable but as a solution, in order to main an adequate OSNR sufficient to monitor wavelength shifts, it is essential to maintain the best possible coupling between the micro-resonator and the tapered.

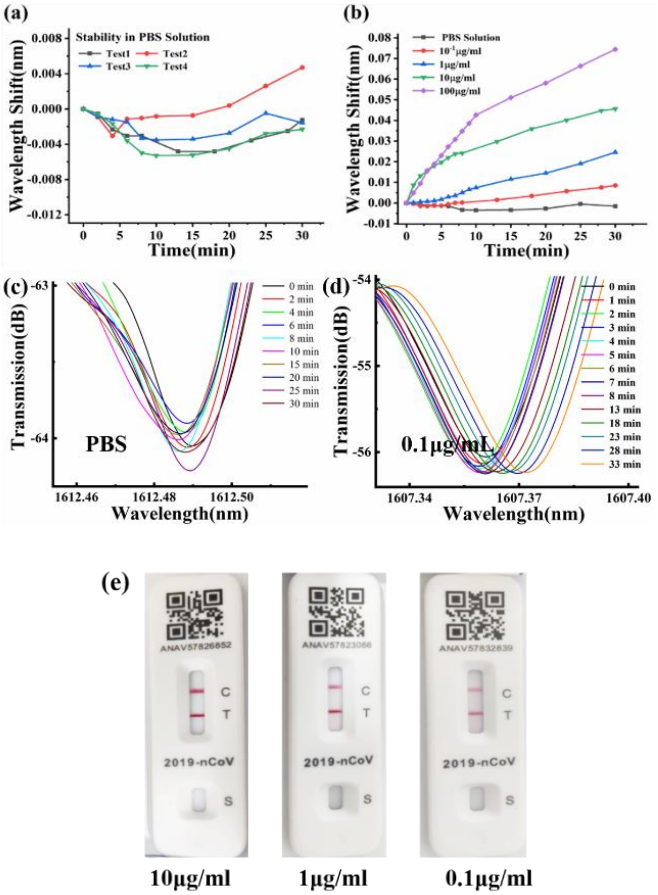

Fig. 8(a) Stability test results of PBS solution; (b) Response of wavelength with time for different N-Protein antigen concentrations; (c) The transmission spectra in PBS; (d) The transmission spectra in N protein with a concentration of 0.1 µg/mL; (e) Antigen detection at different concentrations.

A biomolecular assay was performed for four different concentrations (10^{-1}, 1, 10 and 10^2 µg/mL, Beijing Bersee Science and Technology Co. Ltd.) of the novel coronavirus N-protein antigen. The stability of CMR has been measured in PBS between each test of N protein. During this procedure the transmission dip wavelength was monitored and measured using the OSA. The red-shift of the wavelength dip is mainly generated by binding between the N-Protein antigen molecules and the antibodies of the CMR, which in turn results in a change in the surrounding RI of the resonator. Figure 8(b) plots the correlation between the wavelength shift of the biosensor and the concentration of N-Protein antigen as a function of time. The response for PBS only is also shown for reference. It is observed that the red-shift of the resonance wavelength increases as the N-Protein antigen concentration changes from the lowest value (10^{-1} µg/mL) to the highest value (10^2 µg/mL). The transmission spectra in PBS and in N-Protein with a concentration of 0.1 µg/mL are shown in Figure 8(c) and Figure 8(d), respectively.

For comparison, three of the sample formulations (10 µg/mL, 1 µg/mL and 10^{-1} µg/mL) were also tested using a conventional coronavirus (2019-nCoV) antigen test kit (latex method) (Flowflex, Aikang Biotechnology (Hangzhou) Co., Ltd.). As indicated in Figure 8(e), the color of the T-line (positive test indication) gradually becomes lighter as the concentrations of different N-Proteins were reduced from 10 µg/mL, to 10^{-1} µg/mL.

To further in detail illustrate how the sensor responds to the presence of N-Protein, Figure 9(a) shows the spectra of the functional CMR (containing 100 µg/ml N-Protein-mAb) immersed in 10 µg/mL N-Protein antigen solution over a period of time. It can be seen that the resonance wavelength of the sensor undergoes a red-shift with time. To help to better understand the change of the resonance wavelength during detection, Figure 9(b) shows the resonance wavelength shift over time for the three sensor samples, with the variations between sensors shown error bars, A large proportion of the shift occurs and it occurs in the initial 7 minutes, and the wavelength shifts more slowly over the subsequent 25 minutes. This may be caused by the small size of the N-Protein.

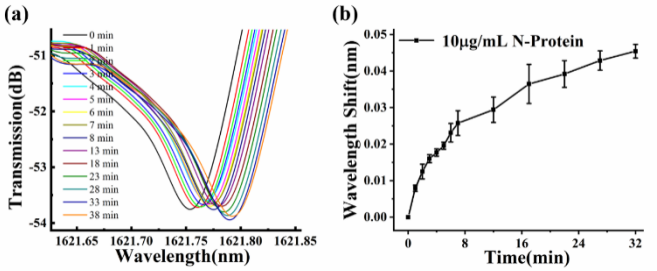

Fig. 9(a) Response of the spectrum over time when the sensor is immersed in N-Protein antigen (10 µg/mL) solution; (b) Response of the spectrum over time and error bars when three experiments are conducted with N-Protein antigen (10 µg/mL) solution.

Sensor reproducibility is a critical parameter for bio-diagnostics. For the purpose of studying the repeatability of the proposed sensor, three sensors were manufactured with identical physical characteristics and surface functionalization conditions. Figure 10(a) shows a histogram the average wavelength shift of the three sensors after 30 minutes following exposure to different N-Protein concentrations. Each error bar is calculated from the standard deviations of the individual shifts for the three sensors. A calibration curve is shown in Figure 10(b) which plots the wavelength shift in relation to the logarithm of the analyte concentration over the concentration range of 10^{-1}-10^{2} µg/mL, along with a linear fit. Based on this calibration curve shown, assuming 3 times of maximum wavelength change in PBS (3×0.005=0.015 nm) is considered as the detection limit, the LoD of the CMR was calculated as approximately 0.23 µg/mL with the R^2 of 0.99. This LoD is better than that for similar sensors based on a microsphere reported previously, such as that in [39] which demonstrated an LoD of 1 µg/ml.

To study the specificity of the sensor to N-Protein, solutions of two different biomolecules were prepared to which the sensor was exposed: S-Protein (10 µg/mL) and tumor necrosis factor (TNF, 10 µg/mL). In each case the sensor was immersed in these solutions and the wavelength shift was measured. The detected wavelength changes for the sensor for these two different biomaterials as a function of time are shown in Fig. 11(a), which also shows the response to PBS for reference. It can be concluded that wavelength shift of the sensor for these two biomaterials is small, almost twenty times lower compared to the shift for N-Protein. This indicates that for the functionalized sensor, binding does not readily take place for biomaterials other than N-Protein molecules.

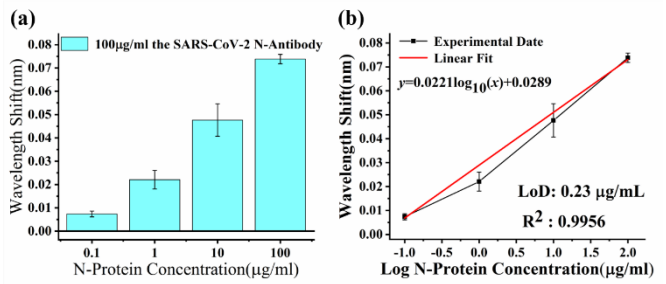

Fig. 10(a) Average wavelength shift with error bars for different concentrations of N-Protein; (b) Calibration curve for N-Protein with concentration range of 10^{-1}-10^{2} µg/mL.

Finally, to simulate a practical application environment, three different types of samples (all using an N-Protein concentration of 10 µg/mL) were prepared and tested. The three samples were: a mixture of S-Protein and N-Protein solution; N-Protein mixed in human saliva and normal human serum (Solarbio, Koitzer Scientific Laboratories). The measured wavelength shifts for the three samples as a function of time are shown in Figure 11(b), along with that for a pure N-Protein sample for comparison. The results show that the sensor has very similar response for all three samples and the pure N-Protein sample, indicating that the sensor has good specificity and could be applied for detecting N-Protein in practical environments.

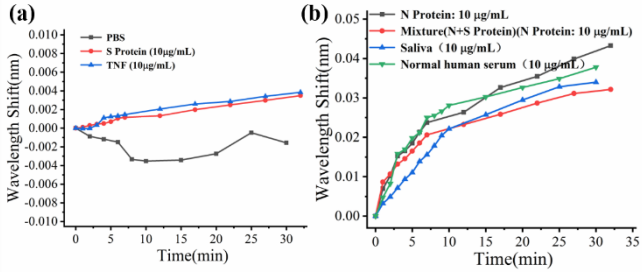

Fig. 11(a)Wavelength shifts when immersing the sensor in S-Protein, TNF and PBS solutions; (b) wavelength shifts for pure N-Protein, mixed solutions (N+S-Protein), saliva and normal human serum solutions.

V. Conclusion

In conclusion, a WGM CMR fiber optic sensor is proposed and experimentally validated for the detection of SARS-CoV-2 N-Protein. Prior to functionalization, experimental measurements indicated that the RI sensitivity of the optical fiber sensor is 75.48 nm/RIU over the RI range 1.3325-1.3415, for the taper waist diameter of 2.76 µm and CMR diameter of 125 µm. The developed CMR was functionalized with 100 µg/mL N-Protein-mAb to detect the

presence of N-Protein. The results showed an LoD of 0.23 ug/mL. Additionally, to study specificity of the sensor, the micro-resonator was immersed in solutions of TNF, S-Protein and also the mixed solution of N-Protein (10 μg/mL) in S-Protein, human saliva, and normal human serum to study the specificity of the CMR. It is shown that the presented biological sensors exhibit excellent repeatability and specificity, and has many possibilities for medical diagnostics and laboratory research applications.

REFERENCES

[1] Gupta P, Goyal K, Kanta P, Ghosh, A, and Singh, MP, “Novel 2019-Coronavirus on New Year's Eve”, Indian Journal of Medical Microbiology, vol. 37, pp. 459-477, Oct. 2019.

[2] T. Li, L. Wang, H. Wang, X. Li, S. Zhang, Y. Xu, and W. Wei, "Serum SARS-COV-2 nucleocapsid protein: a sensitivity and specificity early diagnostic marker for SARS-COV-2 infection", Frontiers in cellular and infection microbiology vol.10, pp. 470, Sep. 2020.

[3] E. Wu, X. Zhang, Y. Zheng, Z. Luo, W. Zhai, Z. Yin, D. Chen, Z. Wang, J. Zhai, Y. Han, H. Liu, R. Li, Y. Wang, Y. Feng, G. Shi, and Y. Ma, "Dynamics of Detection of Anti-SARS-CoV-2 IgG/IgM and SARS-CoV-2 RNA in Respiratory Tract Specimens in 48 COVID-19 Patients." Clinical Laboratory, vol. 67, pp. 2400-2406, Nov. 2021.

[4] H. Zhao, F. Liu, W. Xie, T. Zhou, J. Yang, L. Jin, H. Li, C. Zhao, L. Zhang, J. Wei, Y. Zhang, C. Li, "Ultrasensitive supersandwich-type electrochemical sensor for SARS-CoV-2 from the infected COVID-19 patients using a smartphone," Sensors and Actuators B: Chemical, vol. 327, pp. 128899, Jan. 2021.

[5] A. Yakoh, U. Pimpitak, S. Rengpipat, N. Hirankarn, O. Chailapakul, S. Chaiyo, "based electrochemical biosensor for diagnosing COVID-19: Detection of SARS-CoV-2 antibodies and antigen." Biosensors and Bioelectronics, vol. 176, pp. 112912, Mar. 2021.

[6] SL. Lee, J Kim, S. Choi, J. Han, G. Seo, YW. Lee, "Fiber-optic label-free biosensor for SARS-CoV-2 spike protein detection using biofunctionalized long-period fiber grating," Talanta, vol. 235, pp. 122801, Jul. 2021.

[7] N. Cennamo, L. Pasquardini, F. Arcadio, L. Lunelli, L. Vanzetti, V. Carafa, L. Altucci, L. Zeni, “SARS-CoV-2 spike protein detection through a plasmonic D-shaped plastic optical fiber aptasensor,” Talanta, vol. 233, pp. 122532, Oct. 2021.

[8] JH. Lee, Y. Lee, SK. Lee, J. Kim, CS. Lee, NH. Kim, HG. Kim, "Versatile role of ACE2-based biosensors for detection of SARS-CoV-2 variants and neutralizing antibodies," Biosensors and Bioelectronics, vol. 203, pp. 114034, May. 2022.

[9] AC. Walls, YJ. Park, MA. Tortorici, A. Wall, AT. McGuire, and D. Veesler, "Structure, function, and antigenicity of the SARS-CoV-2 spike glycoprotein." Cell, vol. 181, pp. 281-292, Mar. 2020.

[10] A. Antonopoulos, S. Broome, V. Sharov, C. Ziegenfuss, RL. Easton, M. Panico, A. Dell, HR. Morris, and SM. Haslam, "Site-specific characterization of SARS-CoV-2 spike glycoprotein receptor-binding domain." Glycobiology, vol. 31, pp. 181-187, Aug. 2021.

[11] K. Behrouzi, and L. Lin, "Gold nanoparticle based plasmonic sensing for the detection of SARS-CoV-2 nucleocapsid proteins," Biosensors and Bioelectronics, vol. 195, pp. 113669, Jan. 2022.

[12] A. Lyua, T. Jin, S. Wang, X. Huang, W. Zeng, R. Yang, and H. Cui, "Automatic label-free immunoassay with high sensitivity for rapid detection of SARS-CoV-2 nucleocapsid protein based on chemiluminescent magnetic beads," Sensors and Actuators B: Chemical, vol. 349, pp. 130739, Dec. 2021.

[13] H. Cho, S. Shim, W. Cho, S. Cho, H. Baek, SM. Lee, and DS. Shin, "Electrochemical Impedance-Based Biosensors for the Label-Free Detection of the Nucleocapsid Protein from SARS-CoV-2," ACS sensors, Vol.7, pp. 1676–1684, Jun. 2022.

[14] R. Kumar, Y. Leng, B. Liu, J. Zhou, L. Shao, J. Yuan, X. Fang, S. Wan, T. Wu, J. Liu, R. Binns, Y. Fu, W. Ng, G. Farrell, Y. Semenova, H. Xu, Y. Xiong, X. He, Q. Wu, "Ultrasensitive biosensor based on magnetic microspheres enhanced microfiber interferometer," Biosensors and Bioelectronics, vol.145, pp. 111563, Dec. 2019.

[15] Q. Wu, Y. Qu, J. Liu, J. Yuan, S. Wan, T. Wu, X. He, B. Liu, D. Liu, Y. Ma, Y. Semenova, P. Wang, X. Xin, and G. Farrell, "Singlemode-multimode-singlemode fiber structures for sensing applications—A review," IEEE Sensors Journal, vol.21, pp. 12734-12751, Nov. 2020.

[16] YL. Wang, B. Liu, YN. Pang, J. Liu, JL. Shi, SP. Wan, XD. He, JH. Yuan, and Q. Wu, "Low-cost wearable sensor based on a D-shaped plastic optical fiber for respiration monitoring," IEEE Transactions on Instrumentation and Measurement, vol.70, pp. 1-8, Apr. 2021.

[17] L. Chen, YK. Leng, B. Liu, J. Liu, SP. Wan, T. Wu, JH. Yuan, LY. Shao, GQ. Gu, YQ. Fu, HY. Xu, YH. Xiong, XD. He, and Q. Wu, "Ultrahigh-sensitivity label-free optical fiber biosensor based on a tapered singlemode-no core-singlemode coupler for Staphylococcus aureus detection," Sensors and Actuators B: Chemical, vol.320, pp. 128283, Oct. 2020.

[18] P. Zhang, B. Liu, J. Liu, CF. Xie, SP. Wan, XD. He, XP. Zhang, and Q. Wu, "Investigation of a side-polished fiber MZI and its sensing performance," IEEE Sensors Journal, vol.20, pp. 5909-5914, Feb. 2020.

[19] M. Divagar, R. Gayathri, R. Rasool, J. K. Shamlee, H. Bhatia, J. Satija, and V. V. R. Sai, "Plasmonic Fiberoptic Absorbance Biosensor (P-FAB) for Rapid Detection of SARS-CoV-2 Nucleocapsid Protein." IEEE sensors journal, vol.21, pp. 22758-22766, Aug. 2021.

[20] H. Jia, A. Zhang, Y. Yang, Y. Cui, J. Xu, H. Jiang, S. Tao, D. Zhang, H. Zeng, Z. Hou, and J. Feng, "A graphene oxide coated tapered microfiber acting as a super-sensor for rapid detection of SARS-CoV-2," Lab on a Chip, vol.21, pp. 2398-2406, Apr. 2021.

[21] DK. Agarwal, V. Nandwana, SE. Henrich, Vara Prasad V.N.Josyula, C. ShadThaxton, C. Qi, LM. Simons, JF. Hultquist, EA. Ozer, GS. Shekhawat, and VP. Dravid, "Highly sensitive and ultra-rapid antigen-based detection of SARS-CoV-2 using nanomechanical sensor platform," Biosensors and Bioelectronics, vol. 195, pp. 113647, Jan. 2022.

[22] R. Duan, X. Hao, Y. Li, and H. Li, "Detection of acetylcholinesterase and its inhibitors by liquid crystal biosensor based on whispering gallery mode," Sensors and Actuators B: Chemical, vol. 308, pp. 127672, Apr. 2020.

[23] Y. Wang, H. Zhang, S. Duan, W. Lin, B. Liu, and J. Wu, "Label-free in-situ detection for DNA hybridization employing grapefruit-microstructured-optical-fiber-based microfluidic whispering gallery mode resonator," IEEE Sensors Journal, Vol.21, pp. 9148-9154, Dec.2020.

[24] JA. Freile, G. Choukrani, K. Zimmermann, E. Bremer, and L. Dähne, "Whispering Gallery Modes-based biosensors for real-time monitoring and binding characterization of antibody-based cancer immunotherapeutics," Sensors and Actuators B: Chemical, vol. 346, pp. 130512, Nov. 2021.

[25] Y. Hao and Z. Guo, "Monitor in situ superconducting temperature via optical whispering-gallery mode sensors," Journal of Physics D: Applied Physics, Vol. 52, pp. 175101, Feb. 2019.

[26] Y. Liu, Q. Xia, H. Wang, A. Zhou, Z. Xu, and L. Yuan, "Robust whispering gallery mode resonator for humidity measurement." Optical Fiber Technology, Vol. 60, pp. 102378, Dec. 2020.

[27] N. Bavili, T. Balkan, B. Morova, M. Eryürek, Y. Uysallı, S. Kaya, and A. Kiraz, "Highly sensitive optical sensor for hydrogen gas based on a polymer micro-column ring resonator." Sensors and Actuators B: Chemical, Vol. 310, pp. 127806, May. 2020.

[28] J. Wu, B. Wang, B. Song, M. Qiao, B. Liu, H. Zhang, W. Lin, S. Duan, "Bioimmunoassay based on hydrophobin HGFI self-assembled whispering gallery mode optofluidic microresonator," Sensors and actuators A: physical, vol. 319, 112545, Jan. 2021.

[29] A. Ramachandran, S.Wang, J.Clarke, S.J.Ja, D.Goad, L.Wald, E.M.Flood, E.Knobbe, J.V.Hryniewicz, S.T.Chu, D.Gill, W.Chen, O.King, and B.E. Little, "A universal biosensing platform based on optical micro-ring resonators," Biosensors and Bioelectronics, Vol. 23, pp. 939-944, Feb. 2008.

[30] T. Tajiri, S. Matsumoto, T. Imato, T. Okamoto, and M. Haraguchi, "Optical Characterization of the Antigen–Antibody Thin Layer Using the Whispering Gallery Mode," Analytical Sciences, Vol. 30, pp. 799-804, Jun. 2014.

[31] ST. Hsieh, JE. Cheeney, X. Ding, NV. Myung, and ED. Haberer, "Near-field Electrospinning of Polymer/Phage Whispering Gallery Mode Microfiber Resonators for Label-free Biosensing," Sensors and Actuators B: Chemical, Vol.367, pp. 132062, Sep. 2022.

[32] M. Sumetsky, "Localization of light in optical fibers: Cylinder, conical and bottle microresonators." 2011 13th International Conference on Transparent Optical Networks. IEEE, pp. 1-4, Jun. 2011.

[33] M. Sumetsky, "Whispering gallery modes in a microfiber coil with an n-fold helical symmetry: classical dynamics, stochasticity, long period gratings, and wave parametric resonance," Optics Express, Vol.18, pp. 2413-2425, Jan. 2010.
[34] O. Schwelb, "Transmission, group delay, and dispersion in single-ring optical resonators and add/drop filters-a tutorial overview," Journal of Lightwave Technology, vol.22, pp. 1380-1394, May. 2004.
[35] H. Haus, W. Huang, S. Kawakami, and N. Whitaker, "Coupled-mode theory of optical waveguides," Journal of lightwave technology, vol.5, pp. 16-23, Jan. 1987.
[36] M. Sumetsky, "Mode localization and the Q-factor of a cylindrical microresonator," Optics letters, vol.35, pp. 2385-2387, Jun. 2010.
[37] L Chen, YK Leng, S Qiu, B. Liu, J. Liu, SP. Wan, T. Wu, HY. Xu, YH. Xiong, JH. Yuan, XJ. Xin, DL. Wang, XD. He, Q. Wu. "Ultrahigh-sensitivity label-free singlemode-tapered no core-singlemode fiber immunosensor for Listeria monocytogenes detection." Sensors and Actuators B: Chemical, vol.376, pp. 132930, Feb. 2023.
[38] L Cai, Y Zhao, X Li. "A fiber ring cavity laser sensor for refractive index and temperature measurement with core-offset modal interferometer as tunable filter." Sensors and Actuators B: Chemical, vol.242, pp. 673-678, Apr. 2017.
[39] Y Yue, H Ding and C Chen. "Label-free optical antibody testing kit based on a self-assembled whispering-gallery-mode microsphere." Journal of Biophotonics, vol.14, pp. e202000338, Nov. 2021.

Ru-Lei Xia is a graduate student with the School of Testing and Optical Engineering, Nanchang Hangkong University. Here he mainly studies the application of optical biosensors.

Bin Liu (Member, IEEE) received the B.S. and Ph.D. degrees from Sun Yat-sen University, China. Dr. Liu is an Associate Professor with the Key Laboratory of Opto-Electronic Information Science and Technology of Jiangxi Province, Nanchang Hangkong University, China. He has over 80 publications in the area of photonics and holds 10 invention patents. His current research interests include optical fiber interferometer and the application for sensing, fiber bio-chemical sensors, optical micro-cavity and the application for sensing, surface plasmon resonant, Design and application of micro-nano photonic devices, optical nonlinearity and optical soliton, FBG sensing and distributed fiber sensing.

Yingying Hu received her Ph.D. degree from University of Science and Technology of China, China. She is a lecture with Key Laboratory of Nondestructive Test (Ministry of Education) of Nanchang Hangkong University, China. Her main research interest is fiber optic sensing and qantum random number.

Juan Liu received her Ph.D. degree from Beijing Normal University, China. She is a lecture with Key Laboratory of Nondestructive Test (Ministry of Education) of Nanchang Hangkong University, China. Her main research interest is fiber optic sensing.

Yue Fu is a lecturer with the Key Laboratory of Opto-Electronic Information Science and Technology of Jiangxi Province, Nanchang Hangkong University, China. Her current research interests include ultrasonic detection and photoelectric detection.

Xing-Dao He was born in Jingan, China, in 1963. He received the Ph.D. degree in optics from Beijing Normal University, Beijing, China, in 2005. He is currently a Professor with the Key Laboratory of Nondestructive Test (Ministry of Education), Nanchang Hangkong University, China. His current research interests include light scattering spectroscopy, optical holography, and information processing.

Ping Lu received the master's and doctor's degrees from the Huazhong University of Science and Technology, Wuhan, China, in 1999 and 2005, respectively. She has been a Professor with the College of Optical and Electronic Information, Huazhong University of Science and Technology, since 2011. In 2009, she was with the Arizona Optical Center in America as a Visiting Scholar for one year. She has been a Professor with the College of Optical and Electronic Information, Huazhong University of Science and Technology, since 2011. Her current research interests include optical fiber communication, optical fiber sensing, fiber lasers, and optical waveguide technology.

Gerald Farrell received an MSc on optical receiver design and a PhD from Trinity College Dublin on all-optical clock synchronization using self-pulsating laser diodes. He founded the TU Dublin Photonics Research Centre in 1995, where he led a team of postdoctoral and doctoral researchers. His main research interests are in optical fiber sensing, including sensors for structural health monitoring, chemical and bio-sensors, which use a variety of sensor structures such as fibre hetrostructures, micro-fibers and fibre based microresonators. Prof. Farrell has over 420 journal and conference publications in the area of photonics and has led several long-term research collaborations with research groups in Poland and Australia and China. Prof. Farrell is an experienced doctoral supervisor; has been involved in a number of photonics research networks; a visiting professor at a number of Universities and a Director for several years with the startup company PX Instrument Technology.

Jinhui Yuan received the Ph.D. degree in physical electronics from Beijing University of Posts and Telecommunications (BUPT), Beijing, China, in 2011. He is currently a Professor at the Department of computer and communication engineering, University of Science and Technology Beijing (USTB). He was selected as a Hong Kong Scholar at the Photonics Research Centre, Department of Electronic and Information Engineering, The Hong Kong Polytechnic University, in 2013. His current research interests include photonic crystal fibers, silicon waveguide, and optical fiber devices. He is the Senior Members of the IEEE and OSA. He has published over 200 papers in the academic journals and conferences.

Qiang Wu received the B.S. and Ph.D. degrees from Beijing Normal University and Beijing University of Posts and Telecommunications, Beijing, China, in 1996 and 2004, respectively. From 2004 to 2006, he worked as a Senior Research Associate in City University of Hong Kong. From 2006 to 2008, he took up a research associate post in Heriot-Watt University, Edinburgh, U.K. From 2008 to 2014, he worked as a Stokes Lecturer at Photonics Research Centre, Dublin Institute of Technology, Ireland. He is an Associate Professor / Reader with Faculty of Engineering and Environment, Northumbria University, Newcastle Upon Tyne, United Kingdom. His research interests include optical fiber interferometers for novel fiber optical couplers and sensors, nanofiber, microsphere sensors for bio-chemical sensing, the design and fabrication of fiber Bragg grating devices and their applications for sensing, nonlinear fibre optics, surface plasmon resonant and surface acoustic wave sensors. He has over 280 publications in the area of photonics and holds 8 invention patents. He is an Editorial Board Member of Scientific Reports, an Associate Editor for IEEE Sensors Journal and an Academic Editor for Journal of Sensors.